Supporting information

Single-Molecule Level Insight into Nanoscale Environment-Dependent Photophysics in Blends

Rebecca Grollman,[†] Nicole Quist,[†] Alexander Robertson,[†] Jeremy Rath,[†] Balaji Purushothaman,[‡] Michael M. Haley,[§] John E. Anthony,[‡] and Oksana Ostroverkhova*,[†]

[†]*Department of Physics, Oregon State University, Corvallis, OR 97331, United States*

[‡]*Department of Chemistry, University of Kentucky, Lexington, KY 40506, United States*

[§]*Department of Chemistry & Biochemistry and the Materials Science Institute, University of Oregon, Eugene, OR 97403, United States*

Sample Preparation

Samples for single molecule imaging were prepared in a 1% wt solution of PMMA (75,000 m.w., Polysciences, Inc.) in toluene with a fluorophore (F8 TCHS-Pn) concentration of a multiple of 3.4 x 10^{-10} M as discussed below. Acceptor molecules (TIPS-IF or PCBM) were added to achieve varied average acceptor-acceptor separations between molecules based on the molar fraction of the acceptor and PMMA. Glass coverslips were soaked in a detergent and water solution overnight. They were then sonicated for 40 minutes in the detergent/water solution, rinsed thoroughly in deionized water, then dried under N_2. Cleanliness of coverslip, toluene, and PMMA matrix under the same experimental configuration used for single molecule imaging was ensured before proceeding with preparation of samples of interest. All films were spun at 3000 rpm for 50 seconds from 60 µL of solution. The resulting film thickness as measured by the AFM was 19±2 nm.

The following types of spin-cast films were prepared for single molecule imaging: (i) plain F8 TCHS-Pn (donor) at varying concentrations, (ii) F8 TCHS-Pn (donor) with TIPS-IF (acceptor) with varying concentrations of donor molecules and/or different spacings of acceptor molecules, and (iii) F8 TCHS-Pn (donor) with PCBM (acceptor) with different spacings of acceptor molecules. Donor and acceptor molecules were incorporated as guest molecules in a PMMA host. The baseline concentration of F8 TCHS-Pn was 3.4 x 10^{-10} M (denoted as "1x" below). All other donor concentrations used were multiples of the original concentration; the explored donor concentrations ranged between 1x and 1000x, where 1000x corresponds to 3.4 x 10^{-7} M. Average acceptor-acceptor spacing was calculated from

$$V = \frac{M}{N_A \rho_m f}$$

where V is the average volume per molecule, M is the molar mass of the host (PMMA), N_A is Avogadro's number, ρ_m is the mass density of the host, and f is the molar fraction of guest to host. Assuming spherical volume of $4\pi r^3/3$, the average spacing between molecules R is $2r$.[1,2] Samples with average acceptor-acceptor spacing R ranging between 4 and 20 nm were prepared. Only freshly prepared samples were used in experiments. For experiments performed on different days, calibration F8 TCHS-Pn donor-only samples at 1x and 2x donor concentrations were made every day and imaged with the same settings as other samples to ensure day-to-day reproducibility. For each acceptor-acceptor spacing, acceptor-only in

PMMA samples were prepared and imaged with the same settings as other samples to ensure that acceptor molecules do not contribute fluorescent impurities.

Samples similar to those used in single molecule imaging were prepared for FRET measurements but at higher donor and acceptor concentrations such that the average donor-donor (acceptor-acceptor) spacing was 7 nm (3 nm). Three types of films ("bulk" samples) were prepared: (i) F8 TCHS-Pn donor-only, (ii) acceptor only, and (iii) donor-acceptor, all in PMMA.

Experimental Details

Single molecule fluorescence imaging of F8 TCHS-Pn molecules dispersed in PMMA in the absence (in donor-only samples) and in the presence of acceptor molecules was performed under circularly polarized 633 nm wide-field illumination using an Olympus IX-71 inverted microscope with a 100x UPlanSApo (NA 1.4) oil objective and an Andor iXon EMCCD (DU-897) detector. The z633rdc and HQ645LP Chroma Tech filters were used for imaging. Collection efficiency was estimated to be 10.6% as described in our previous publication.[3] An integration time of 100 ms was used, and 100 s videos were collected from various areas of each sample. For selected samples, up to 6 consecutive videos were taken from the same sample area. Potential individual fluorophores were detected using custom MATLAB scripts, and time traces were selected for further analysis if the trace exhibited digital switching behavior.[3]

Because of the significant background, the data are processed using a custom MATLAB program that determines and subtracts the local background for each fluorophore. In particular, the counts acquired during an "off" time period were averaged to determine a background, which was then subtracted from the counts during the "on" time period. Then, the count level for the "off" time periods is zero (Figure 3(a)).

The number of detected photons is related to the EMCCD counts as follows:

Photons detected = counts x AD conversion / (EM Gain).

Here the counts are the EMCCD counts (e.g. in Fig. 3(a)), with the background subtracted, the AD conversion is the analog to digital conversion determined by the EMCCD settings (12.68) and EM gain is set to 40x for all samples.

Optical absorption and photoluminescence (PL) spectra of molecules in toluene and in "bulk" samples were measured using Ocean Optics USB2000 and USB2000-FLG spectrometers, respectively.[4] Changes in PL lifetimes in "bulk" samples due to FRET were measured under 470 ps 532 nm excitation (Q-switched frequency-doubled Nd:YAG, 55 kHz, Altechna STA-01-SH-4-MOPA). A time-correlated single photon counting (TCSPC) board (PicoQuant TimeHarp 200) was used with a single photon avalanche photodiode (SPAD – Molecular Photonic Devices) for detection. The instrument response function (IRF) was recorded using scattered light from a frosted glass slide and was 260 ps. Details of the set up can be found elsewhere.[4]

Concentration vs intermolecular distance calibration

To calibrate our concentrations, we first imaged donor-only samples and monitored how the number of detected F8 TCHS-Pn fluorophores (characterized by the digital two-level switching behavior) scaled with the donor concentration. As expected, the concentration increase from 1x to 2x resulted in a doubled number of the fluorophores behaving as a two-level system (Figure S1). At higher concentrations, however, the scaling did not persist; for example at the 10x concentrations, the number of fluorophores exhibiting the two-level behavior was about the same as at 1x concentrations, and this number progressively decreased as the donor concentration increased (Figure S1). This was accompanied by an increase in traces showing three or more levels. In particular, while less than 10% of all time trajectories with a single-step ("digital") switching exhibited a three-level behavior at a 1x donor concentration, the number increased to about 80% at a 100x donor concentration. This is due to two donor molecules spaced at a distance within the diffraction-limited spot (i.e. <230 nm) contributing to the same time trace. At donor concentrations of 500x and 1000x, only a few incidences of two-level behavior were observed.

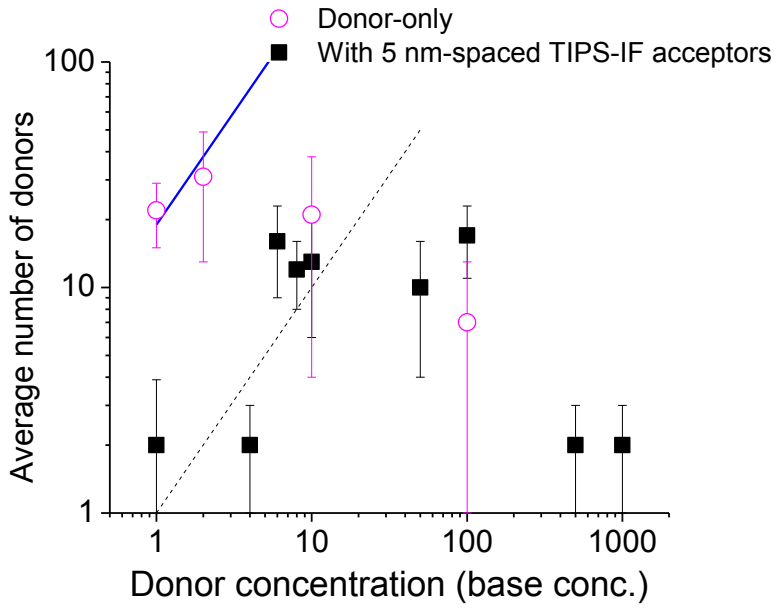

Figure S1. Average number of detected F8 TCHS-Pn molecules (characterized by two-level digital-switching time trajectories) in the field of view depending on the donor concentration, in donor-only samples and in donor-acceptor samples with 5 nm-spaced TIPS-IF acceptors. The donor concentration is given in terms of the base concentration which is 3.4×10^{-10} M. Error bars correspond to variations in the fluorophore numbers in different areas of the sample. Lines show expected scaling behavior at low concentrations, in donor-only (blue) and donor-acceptor (black) samples, when the average donor-donor separation is considerably higher than the minimal separation resolved within the diffraction limit.

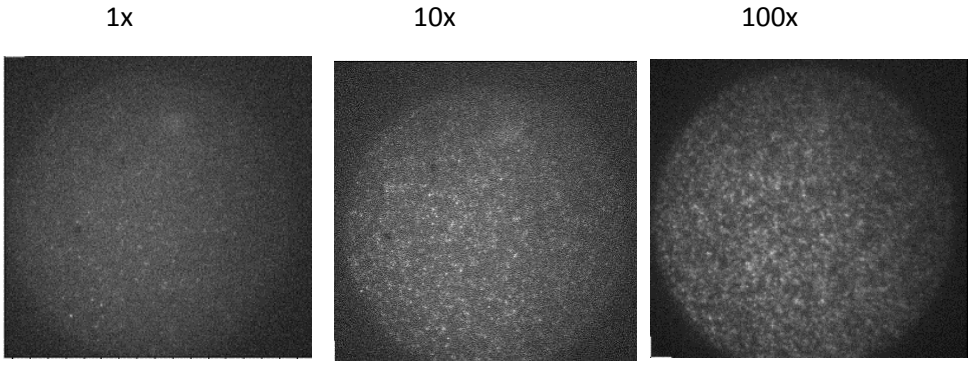

Figure S2. Wide-field images of F8 TCHS-Pn in PMMA (donor-only) in samples prepared with 1x, 10x, and 100x donor concentrations. In our analysis of these images, many fluorophores visible to the eye are rejected by our MATLAB script due to rigorous fluorophore selection standards specifically requiring a well-defined behavior of a two-level system. These rejected fluorophores were either nanoaggregates (in samples with higher donor concentrations) or a population of fluorophores that did not exhibit any blinking or did not turn "off" over the duration of the video.

Next, we probed how the number of detected F8 TCHS-Pn donors changes in the presence of TIPS-IF acceptors at various average acceptor-acceptor spacings, depending on the donor concentration. As the acceptor loading increased (so that the average acceptor-acceptor spacing decreased from 20 nm to 5 nm), the average number of fluorophores in the field of view remained the same until ~6 nm and then rapidly diminished at 5 nm. At 5 nm acceptor-acceptor spacing, very low numbers of fluorophores were detected in samples with the 1x-4x donor concentrations, due to efficient donor-acceptor FRET that quenched the F8 TCHS-Pn fluorescence at time scales considerably below those resolved in our single molecule imaging experiments. Therefore, donor concentrations of at least 6x were used, and the donor concentrations in the 6x -100x range were proven to be usable for 5 nm-spaced acceptor samples (Figure S3). At higher donor concentrations (such as 100x), FRET acts a super-resolution mechanism that enables single-molecule-level detection even though there are several fluorescent molecules within the diffraction-limited image area as can be appreciated from Figure S1. This manifests in a dramatic reduction in the percentage of multiple-level time trajectories in comparison with that in donor-only samples. For example, at 100x donor concentration and with 5 nm-spaced TIPS-IF acceptors, only ~20% of all time traces were multiple-level trajectories, which is considerably lower than ~80% observed in donor-only samples with the same donor concentration. Samples with 3 and 4 nm average acceptor-acceptor spacing were also prepared, however an increased fluorescence background in these samples prevented reliable quantitative analysis of the fluorescence time trajectories, which limited our quantitative studies to the samples with ≥ 5 nm acceptor-acceptor spacing.

Images illustrating effects of FRET are shown in Figure S3. The fluorophores that are within the FRET radius from a nearest acceptor appear dark in our measurements. Similar results were obtained with PCBM acceptors which also efficiently quenched fluorescence of the F8 TCHS-Pn molecules (Figure S4).

10x (donor-only)

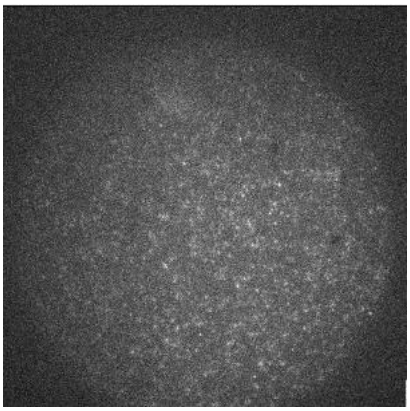

10x donor + 5 nm-spaced TIPS-IF acceptors

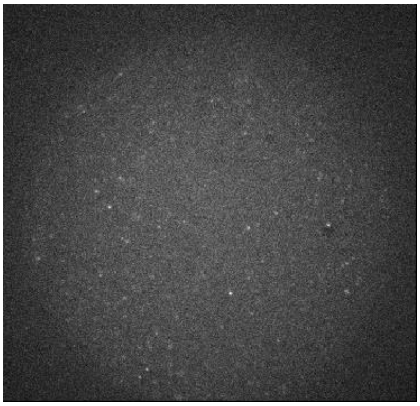

100x (donor-only)

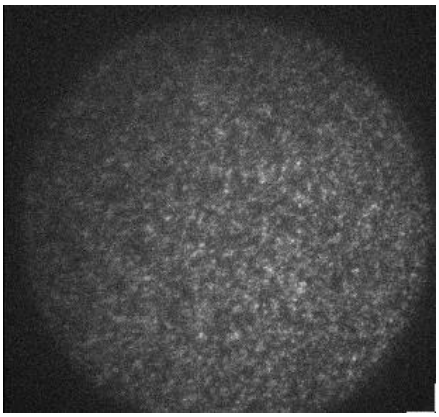

100x donor + 5 nm-spaced TIPS-IF acceptors

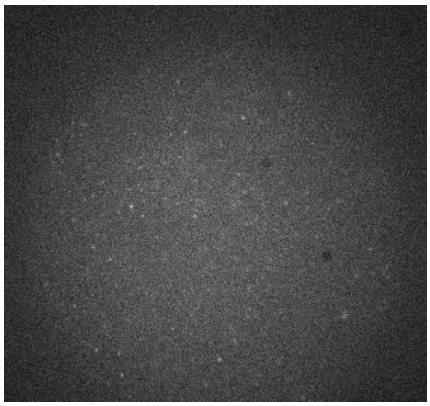

Figure S3. Wide-field fluorescence images from donor-only and donor-acceptor (with 5 nm-spaced acceptors) samples at 10x and 100x donor concentrations.

FRET radius calculations

The FRET radius was calculated using both the "bulk" approach and the single-molecule approach, as described below.

The "bulk" approach relied on measurements of the donor emission and acceptor absorption spectra and donor fluorescence quantum yield (QY) measured at low concentrations of donor or acceptor molecules dispersed in PMMA, as described in our previous publications.[2,3] The FRET radius R_0 was calculated according to[3]

$$R_0^6 = \frac{9\ln(10)}{128\,\pi^5 N_A}\frac{\kappa^2 \Phi_F}{n^4} J,$$

where *J* is the overlap integral given by

$$J = \int_0^\infty F_d(\lambda)\varepsilon_a(\lambda)\lambda^4 d\lambda,$$

n is the index of refraction of the host material (PMMA), Φ_F is the fluorescence QY of the donor (F8 TCHS-Pn) in PMMA, N_A is Avogadro's number, $F_d(\lambda)$ is the normalized fluorescence spectrum of the donor, $\varepsilon_a(\lambda)$ is the molar extinction coefficient of the acceptor, and κ is the dipole orientation factor. It is taken to be $\kappa = 0.845\sqrt{2/3}$ (static isotropic average) for an ensemble of acceptors that are statistically randomly distributed about the donor with respect to both distance and orientation in a rigid medium.[3] This approach yielded R_0 of 2.7 nm and 3.4 nm for the case of TIPS-IF and PCBM acceptors, respectively.

The single-molecule approach involved the dependence of the number of detected fluorophores depending on the average acceptor-acceptor spacing shown in Fig. 2(b). As the sharp drop-off in the number of fluorophores at <6 nm acceptor-acceptor spacing is attributed to FRET, we fit the observed dependence with

$N_D = N_0/(1+(R_0/R)^6)$

where N_D is the number of single molecule donors in the donor-acceptor samples, R is the average acceptor-acceptor separation divided by 2 (assuming that the donor is located at half the distance between the acceptors), N_0 is the number of single molecule donors with no acceptors present, and R_0 is the FRET radius. With this fit, the FRET radius for F8 TCHS-Pn and TIPS-IF (PCBM) was estimated to be 3.1± 0.3 nm (3.9± 0.4 nm), trending with the corresponding FRET radii calculated using the "bulk" approach.

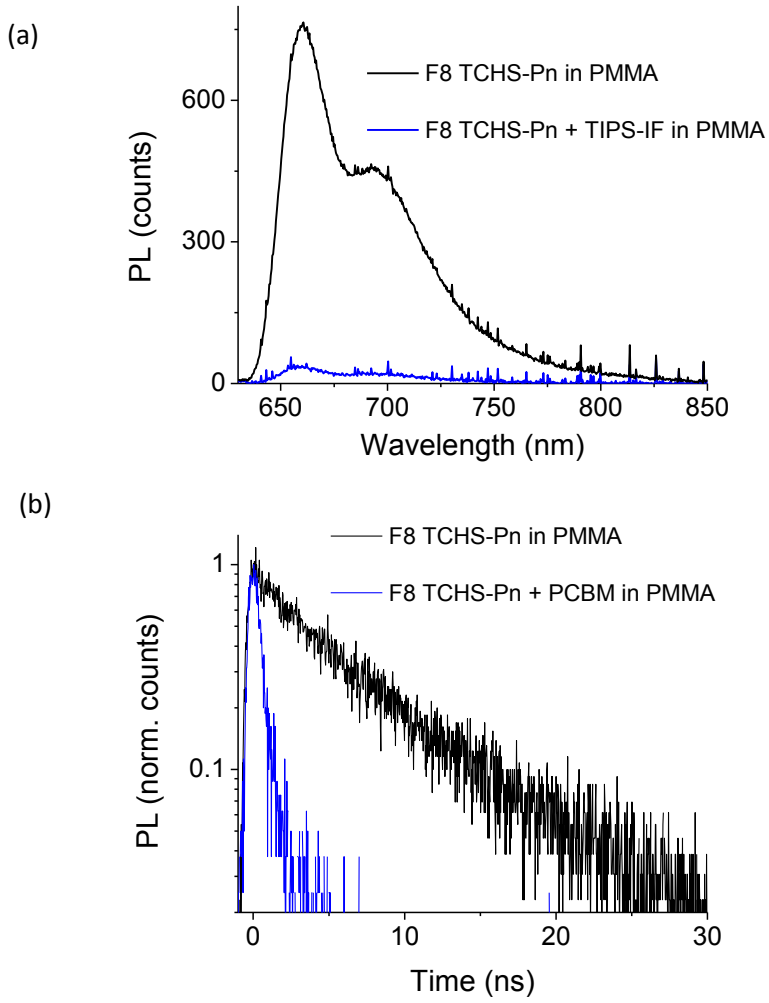

Figure S4. (a) Photoluminescence (PL) spectra for F8 TCHS-Pn donor emission from samples with low concentrations of F8 TCHS-Pn in donor-only and in donor-acceptor "bulk" samples in PMMA under 633 nm excitation. Dramatic quenching of the F8 TCHS-Pn PL is observed in donor-acceptor samples due to FRET; the TIPS-IF acceptors are not emissive under these conditions. (b) PL lifetime decay of the F8 TCHS-Pn donor emission in donor-only and donor-acceptor "bulk" samples with PCBM acceptor. Fast quenching due to efficient FRET is observed in the donor-acceptor sample.

Complementary Cumulative Distribution Function (CCDF) analysis

For the CCDF analysis, the built-in MLE function in MATLAB, and the following CDF fit functions were used:

$$S_{PL}(t) = 1 - \left(\frac{t}{t_{min}}\right)^{1-A}$$

$$S_{LN}(t) = \frac{1}{2} erfc\left(\frac{-1}{\sqrt{2}} \frac{\ln(t) - \mu}{\sigma}\right)$$

$$S_{EXP}(t) = 1 - e^{-\lambda t}$$

$$S_{WB}(t) = 1 - e^{-\left(\frac{t}{\beta}\right)^{A}}$$

where S_{PL}, S_{LN}, S_{EXP}, and S_{WB} are the CDFs for power law, lognormal, exponential, and Weibull respectively. The CCDFs were calculated from 1 – S(t).

Table S1. Examples of data sets under study and the number of fluorophores used in analysis of each data set. Each data set was taken on a separate day.

Sample	Data set number	Number of fluorophores analyzed
Donor-only 1x	1	289
Donor-only 2x	1	358
Donor (1x)-acceptor; 10 nm TIPS-IF	1	187
Donor(1x) -acceptor; 9 nm TIPS-IF	1	225
Donor (1x)-acceptor; 8 nm TIPS-IF	1	308
Donor-only 2x	2	290
Donor (6x) -acceptor; 5 nm TIPS-IF	2	249
Donor (10x) -acceptor; 5 nm TIPS-IF	2	182
Donor (50x) -acceptor; 5 nm TIPS-IF	2	115
Donor-only 2x	3	334
Donor (1x)-acceptor; 10 nm PCBM	3	287
Donor (1x)-acceptor; 9 nm PCBM	3	151
Donor-only 1x	4	264
Donor-only 2x	4	358
Donor-only 10x	4	253
Donor (1x)-acceptor; 7 nm TIPS-IF	4	142
Donor (1x)-acceptor; 6 nm TIPS-IF	4	171

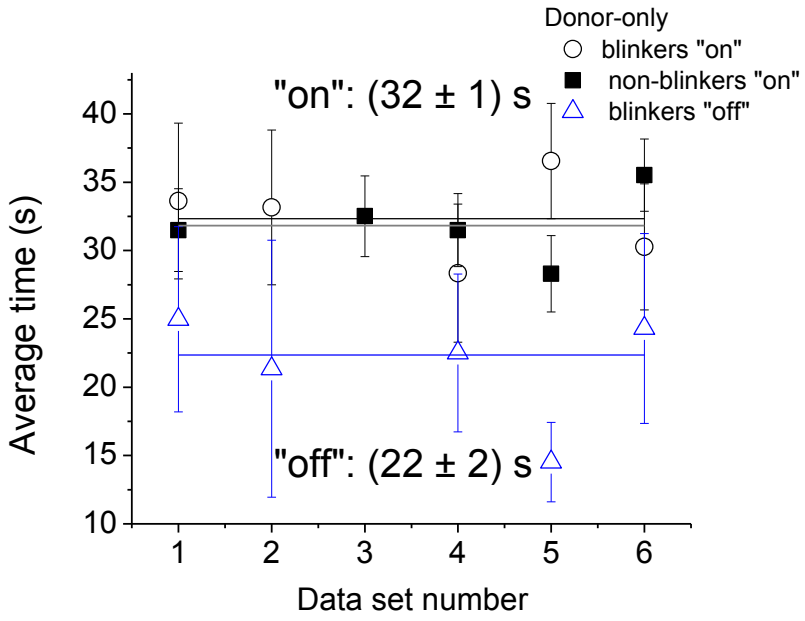

Figure S5. Average "on" and "off" time durations calculated from Weibull fit parameters for donor-only samples measured on different days (represented by data set numbers). Error bars correspond to variation in values obtained from different areas of the same sample. The lines are fits to a constant. The average "on" time durations for "blinkers" and "non-blinkers" were similar within the error.

Monte Carlo simulations

To develop a better understanding of how the Weibull-distributed distributions are created and how various parameters of the model of Fig. 8 affect the resulting CCDFs, we used a Monte Carlo simulation to generate the fluorescence time trajectories.[5] This simulation includes transitions between the ground state (1), the excited state (2), and the dark state (3). Whether the transition between these states occurs is determined by comparing a randomly chosen number between zero and one to the probability of transition between the given state and the new state. The probability of transition is determined by multiplying the transition rate, k_{ij} (s^{-1}), by the time step, dt (s), to determine the probability of transition within that given time. The simulation counts the number of photons that are emitted during the transition from the excited state to the ground state within a 100 ms window. This procedure produces fluorescent time traces (Figure S6) that are comparable to those collected experimentally, which are then processed the same way as our experimental data.

The transition rates chosen for simulations are either determined based on the experimental conditions or the experimental data. For example, the transition rate from the ground state to the excited state k_{12} is calculated from the excitation intensity and the molecular absorption cross section, and the rates k_{21} and k_{21n} are obtained from the fluorescence QY and lifetimes.[3] In comparison, the transition rate from the "dark" state to the ground state, k_{31}, is chosen based on average "off" time duration from our experimental data. With fixed transition rates, the CCDF from the simulated data fits to an exponential distribution, as expected. However, if transition rates evolve with time following a particular time dependence $k \sim t^{A-1}$, then the CCDFs are described by a Weibull distribution ($\exp(-t/\beta)^A$) (Figure S7), as observed in our experimental data.

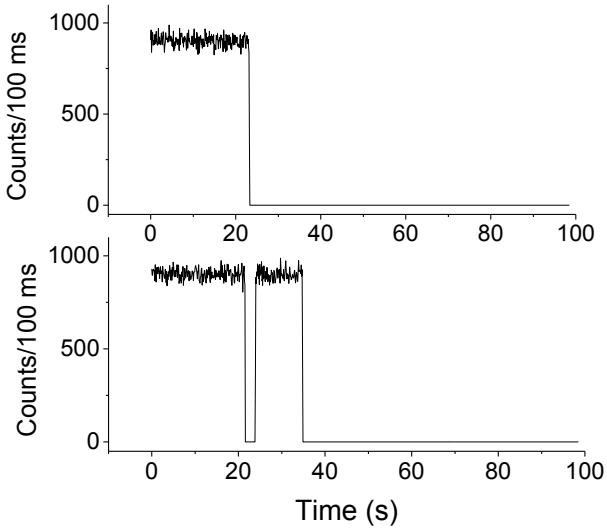

Figure S6. Examples of "nonblinking" and "blinking" time trajectories simulated using Monte Carlo method. The rates (in s^{-1}) used are: k_{12} = 1.1x 10^4, k_{21} = 7x 10^7, k_{21n} = 1.5x10^7, k_{31} = 0.25, k_3= 15, and k_{3w} = 1.5 k_3 $((k_3\,t)^{0.5})$. Here k_{23w} is a Weibull-distributed rate $k = (A/\beta)\,(t/\beta)^{A-1}$ where A and β are Weibull parameters (such that the Weibull CCDF is $\exp[-(t/\beta)^A]$.

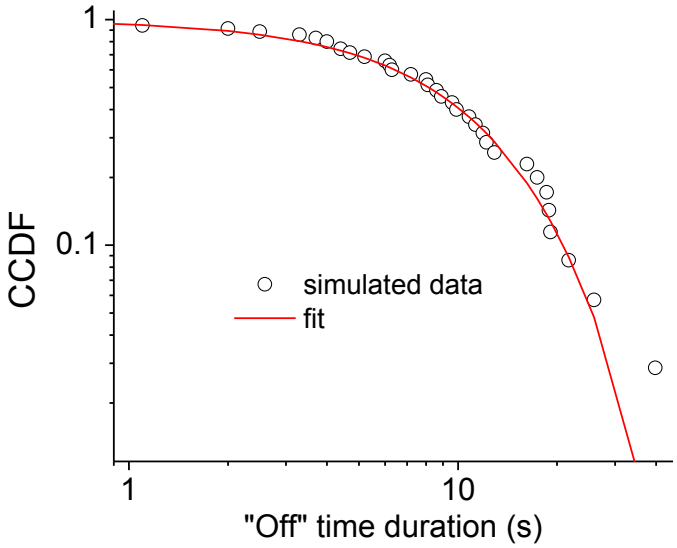

Figure S7. Example of CCDF for the "off" time duration obtained from 200 simulated fluorescence time trajectories, of which 31 exhibited blinking events, such as those shown in Figure S6. The rates (in s^{-1}) used are: k_{12} = 1.1x 10^4, k_{21} = 7x 10^7, k_{21n} = 1.5x10^7, k_3= 15, and k_{31} = 0.05 and k_{31w} = 1.2 k_{31} $((k_3\,t)^{0.2})$. Here k_{31w} is a Weibull-distributed rate that determines the distribution of the "off" time durations, $k = (A/\beta)\,(t/\beta)^{A-1}$ where A and β are Weibull parameters (such that the Weibull CCDF is $\exp[-(t/\beta)^A]$). The simulated data are then processed the same way as the experimental data. The Weibull fit (p = 0.98) is also included.

P-tests

Statistical tests using p-values were performed following a previously published procedure.[6] The p-values were calculated using the Kolmogorov-Smirnov (KS) statistic *D* where

$$D = max_{-\infty<t<\infty}\left|S_{fit}(t) - S(t)\right|$$

and $S_{fit}(t)$ is the CDF with the fit parameters being tested and $S(t)$ is the actual data set. To calculate the p-value, N_s data sets are generated with the fit parameters, and the KS statistic is calculated for each generated data set. The p-value then becomes

$$p - value = \frac{\sum D_{synth} \geq D}{N_s}.$$

Accuracy of the p-value is determined by $1/2\sqrt{N_s}$. As a first test, N_s was set to 100 to determine which fits should be investigated further; then, N_s was then set to 10,000 to obtain more accurate p-values. Power law, lognormal, single exponential, and Weibull fits were tested.[6,7]

Table S2. Results of selected p-tests. The highest p-value is shown in boldface.

				p-values			
CCDF type	**sample**	**#fluorophores**	**N_s**	**Power law**	**Lognormal**	**Exponential**	**Weibull**
Nonblinkers ON	Donor-only	158	100	0	0	0	**0.93**
	10 nm TIPS-IF	104	100	0	0.04	0	**0.47**
	9 nm TIPS-IF	115	100	0	0	0	**0.33**
	8 nm TIPS-IF	195	100	0	0	0	**0.25**
	5 nm TIPS-IF	116	10000	0	0.03	0.01	**0.48**
Blinkers ON	Donor-only	79	100	0	0.57	0	**0.94**
	9 nm TIPS-IF	61	100	0	0.06	0.05	**0.72**
	6 nm TIPS-IF	75	100	0	0.07	0.01	**0.2**
	5 nm TIPS-IF	43	100	0	0.14	0.06	**0.78**
Blinkers OFF	Donor-only	66	10000	0	**0.23**	0.02	0.02
	Donor-only	42	100	0	0.12	0	**0.17**
	20 nm	77	100	0	**0.05**	0.02	0

	TIPS-IF						
	10 nm PCBM	22	100	0	0.08	0.18	**0.43**
	8 nm TIPS-IF	104	100	0	0.04	0.13	**0.27**
	7 nm TIPS-IF	66	100	0	0.02	0.06	**0.19**
	5 nm TIPS-IF	93	10000	0	0.22	0.02	**0.41**
	Donor-only	77	10000	0	**0.09**	0.02	0.05
	6 nm TIPS-IF	75	100	0	**0.33**	0.11	0.14

Table S3. Examples of fit parameters obtained from selected CCDF fits to the Weibull (or Lognormal, when in parenthesis, for the data sets with higher p-values for Lognormal) function.

		Weibull (or Lognormal) fit parameters, $\exp(-t/\beta)^A$ (or 1-(1/2)*erfc*(-(ln(t)-μ)/σ√2)		**Average time**
CCDF type	**Sample**	**A (or σ)**	**β (s) (or μ)**	**$\langle\tau\rangle_{on}$ or $\langle\tau\rangle_{off}$**
Nonblinkers ON	Donor-only	1.34	34.3	31.5
	Donor-only	1.30	35.2	32.5
	Donor-only	1.47	34.8	31.5
	Donor-only	1.48	31.3	28.3
	Donor-only	1.52	39.4	35.3
	20 nm TIPS-IF	1.47	29.8	27.0
	10 nm TIPS-IF	1.44	33.1	30.0
	9 nm TIPS-IF	1.55	40.2	36.1
	8 nm TIPS-IF	1.57	39.7	35.6
	6 nm TIPS-IF	1.39	26.2	23.9
	5 nm TIPS-IF	1.30	21.4	19.8
	5 nm TIPS-IF	1.54	10.1	9.1
	5 nm TIPS-IF	1.40	14.8	13.5
	5 nm TIPS-IF	1.27	15.8	17.6
Blinkers ON	Donor-only	1.79	37.8	33.6
	Donor-only	1.56	36.9	33.1
	Donor-only	1.62	31.7	28.4
	Donor-only	1.91	41.2	36.6
	Donor-only	1.88	34.1	30.3
	20 nm TIPS-IF	1.93	36.2	32.1
	10 nm TIPS-IF	1.80	41.7	37.1
	9 nm TIPS-IF	1.59	37.7	33.8
	5 nm TIPS-IF	1.19	15.7	14.8
	5 nm TIPS-IF	1.46	15.3	13.9

	5 nm TIPS-IF	1.34	14.7	13.5
	5 nm TIPS-IF	1.31	13.7	12.7
Blinkers OFF	Donor-only	1.09	25.8	25.0
	Donor-only	1.2	22.7	21.3
	Donor-only	1.11	23.4	22.5
	Donor-only	1.09	15.0	14.5
	Donor-only	1.02	24.5	24.3
	Donor-only	(0.89)	(2.67)	(21.5)
	20 nm TIPS-IF	1.15	22.1	21.1
	20 nm TIPS-IF	(0.89)	(2.64)	(20.9)
	8 nm TIPS-IF	1.26	31.2	29.0
	7 nm TIPS-IF	1.20	29.0	27.3
	5 nm TIPS-IF	1.52	42.0	37.9

"On" and "off" time duration correlations

To determine the contribution of memory-dependent processes into blinking patterns, we selected time trajectories with well-defined "on" periods (i.e. those not limited by the duration of the video) following the "off" periods as described in the Experimental section. The CCDFs in Figure S8 were created using the same sample sets as those used in Figure 7.

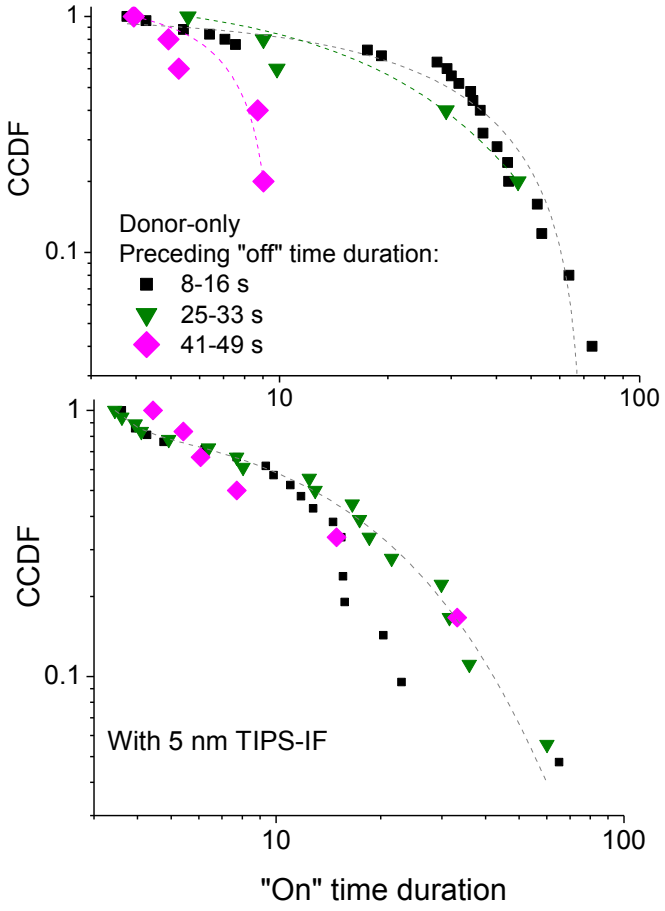

Figure S8. Dependence of the “on” time duration on the preceding “off” time duration in “blinkers” for donor-only samples (top) and donor-acceptor samples with 5 nm-spaced TIPS-IF acceptors. Lines are to guide the eye. In donor-only samples, the probability to observe an “on” time longer than 10 s following an ”off” time considerably decreases as the “off” time duration. No such dramatic dependence of the “on” times on the preceding “off” time duration is observed in donor-acceptor samples at high acceptor concentration.

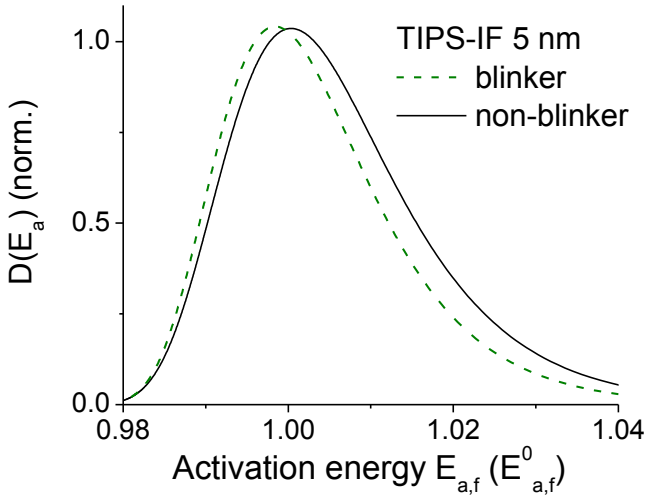

Figure S9. Distributions of activation energies for the forward reaction ($E_{a,f}$) for "non-blinkers" and "blinkers" in donor-acceptor samples with 5 nm-spaced TIPS-IF acceptor. The scale is set with respect to $E^0_{a,f}$ which is the most probable activation energy for forward reactions in "non-blinkers". Considerably smaller difference in the distributions is observed in donor-acceptor samples as compared to donor-only samples (Figure 9(c)).

Photobleaching

The relative photostability of F8 R-Pn derivatives dispersed at low concentrations (which minimize intermolecular interactions between two Pn molecules) in several host matrices has been studied in our previous work.[3] Figure S11 shows a dramatic reduction of photobleaching of F8 TIPS-Pn in PMMA in vacuum, as compared to that in air, highlighting importance of interaction with oxygen in the photobleaching process. The TIPS derivative was found to be the least stable and the TCHS derivative the most stable of all F8 R-Pn derivatives studied.[3]

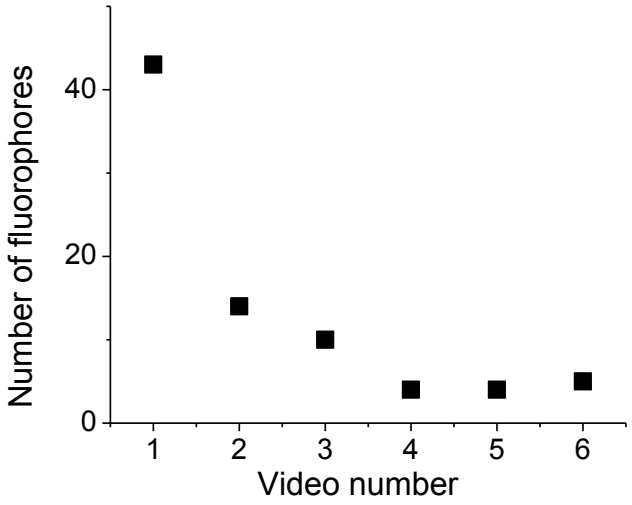

Figure S10. The number of fluorophores (with two-level time trajectories) identified in one sample area over up to 6 consecutive videos. Each video is 100 s duration. The decreasing number of fluorophores in each video demonstrates that the length of 100 s videos used in our experiments captures most of the salient features of the fluorophore photophysics. Vast majority of the fluorophores identified in videos 2 and 3 are a population of molecules that did not exhibit a digital switching behavior in video 1 and were discarded from analysis. The probability of fluorophores considered to be "non-blinkers" in video 1 but turning "on" in subsequent videos is very low.

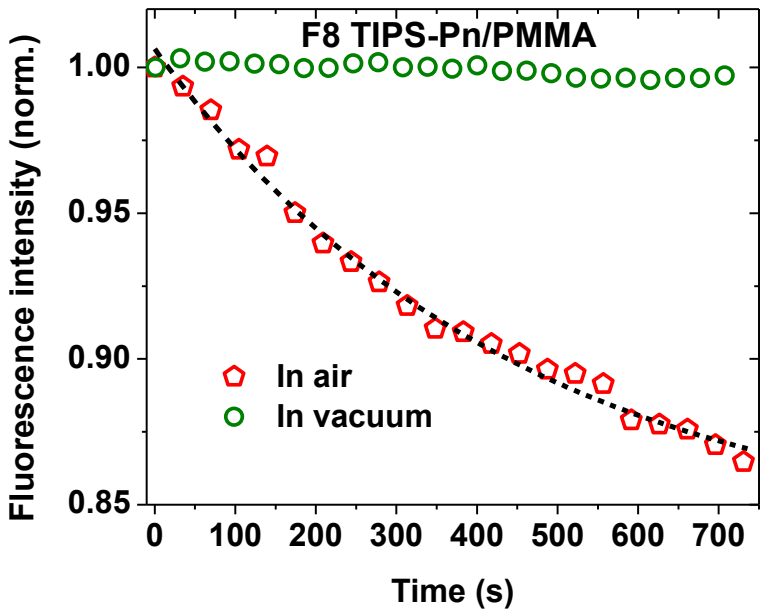

Figure S11. Decay of the fluorescence emission due to photobleaching for F8 TIPS-Pn dispersed at low concentrations in PMMA at 633 nm illumination in air and in vacuum (at 10^{-5} Torr). Line provides a guide for the eye.

References

(1) Shepherd, W. E. B.; Platt, A. D.; Hofer, D.; Ostroverkhova, O.; Loth, M.; Anthony, J. E. Aggregate Formation and Its Effect on (opto)electronic Properties of Guest-Host Organic Semiconductors. *Appl. Phys. Lett.* **2010**, *97* (16), 163303.

(2) Shepherd, W. E. B.; Platt, A. D.; Kendrick, M. J.; Loth, M. A.; Anthony, J. E.; Ostroverkhova, O. Energy Transfer and Exciplex Formation and Their Impact on Exciton and Charge Carrier Dynamics in Organic Films. *J. Phys. Chem. Lett.* **2011**, *2* (5), 362–366.

(3) Shepherd, W. E. B.; Grollman, R.; Robertson, A.; Paudel, K.; Hallani, R.; Loth, M. A.; Anthony, J. E.; Ostroverkhova, O. Single-Molecule Imaging of Organic Semiconductors: Toward Nanoscale Insights into Photophysics and Molecular Packing. *Chem. Phys. Lett.* **2015**, *629*, 29–35.

(4) Platt, A. D.; Day, J.; Subramanian, S.; Anthony, J. E.; Ostroverkhova, O. Optical, Fluorescent, and (photo)conductive Properties of High-Performance Functionalized Pentacene and Anthradithiophene Derivatives. *J. Phys. Chem. C* **2009**, *113* (31), 14006–14014.

(5) Quist, N.; Grollman, R.; Rath, J.; Robertson, A.; Haley, M.; Anthony, J.; Ostroverkhova, O. Single Molecule-Level Study of Donor-Acceptor Interactions and Nanoscale Environment in Blends. *Proc. SPIE* **2017**, *10101*, 101010K.

(6) Riley, E. A.; Hess, C. M.; Whitham, P. J.; Reid, P. J. Beyond Power Laws: A New Approach for Analyzing Single Molecule Photoluminescence Intermittency. *J. Chem. Phys.* **2012**, *136* (18), 184508.

(7) Wong, N.; Ogata, A.; Wustholz, K. Dispersive Electron-Transfer Kinetics from Single Molecules on TiO2 Nanoparticle Films. *J. Phys. Chem. C* **2013**, *117*, 21075–21085.